



A novel EVA-based composite via ceramization toward excellent flame retardance performance and high-temperature resistance

Hong-Wei Di¹ · Chao Fan¹ · Hua He¹ · Nan Zhang¹ · Jun-Ling Dong¹ · Ya-Ting Wang¹

Received: 15 April 2023 / Accepted: 19 August 2023 / Published online: 25 September 2023
© Akadémiai Kiadó, Budapest, Hungary 2023

Abstract

The development of ceramifiable polymer composites is an important means to ensure public safety and meet the emergency operation of power supply lines of public facilities in case of fire. Although there have been many researches on ceramifiable flame-retardant polymer composites and published scientific research achievements, the problem of poor flame-retardant effect of ceramifiable polymer materials due to low flame-retardant efficiency has not been solved. In this study, ethylene–vinyl acetate copolymer (EVA) was used as the matrix, E-glass fiber (EGF) and low softening point glass powder (GP) were selected as the ceramifiable filler (CF), and melamine (MA) and organic modified montmorillonite (OMMT) were used as the complex flame-retardant system. The flame-retardant test results show that when the composition of the composite is EVA/CF (GP:EGF)/MA/OMMT = 35/32 (7:3)/28/5, the flame-retardant property reaches V-0 rating (UL-94), and the corresponding LOI is 27.8. At this time, the bending strength of EVA composite-based ceramic fired at 700 °C reaches 5.1 MPa. TG-IR test results confirmed that a large amount of nonflammable gases from melamine thermal decomposition diluted the combustible gases produced by EVA decomposition, which is the reason why EVA composite has good flame retardancy.

Keywords Polymer-matrix composites (PMCs) · Flame/fire retardancy · Ceramifiable polymer composites · Melamine · Ethylene–vinyl acetate (EVA)

Introduction

As a new type of refractory, ceramicable polymer composite generally includes the following components: polymer substrate, ceramic mineral filler and flux, and flame retardant and other additives. Mineral filler and flux are used as ceramic components to provide material basis for the formation of ceramics. In case of fire, this material is vitrified at high temperature and transformed into a hard ceramic protective layer, which can resist the ablation of thousands of degrees of open fire, and has a certain strength, which can resist water pouring and spraying without cracking [1]. In addition, the ceramic protective layer can also play a role in blocking material exchange and heat transfer, which can not only inhibit the volatilization and loss of materials inside, but also effectively block the diffusion of external heat to

the materials, preventing the spread of fire. Ceramic flame-retardant polymer composites generally use low smoke, non-toxic halogen-free flame retardant, which is a fire-retardant material with excellent performance.

With the progress of society, the requirements of high-temperature resistance, ablation resistance, thermal insulation performance, and mechanical strength of fire-resistant cable in special fire environment are constantly improving, and the research on ceramicized refractory polymer materials has gained attention. Domestic and foreign scholars have carried out a lot of research work on silicone rubber-based ceramifiable composites [2–8]. However, the application of silicone rubber-based ceramifiable composites is limited by the single variety of silicone rubber and poor mechanical properties of the composites and its ceramics. Compared with silicone rubber, ordinary polyolefin materials (such as ethylene–vinyl acetate copolymer (EVA)) have better mechanical properties and can expand the variety of ceramifiable polymer composites. At present, there are some researches on polyolefin-based ceramifiable flame-retardant composites [9–11], and the effect is not ideal. For EVA-based ceramifiable flame-retardant composites [9],

✉ Hong-Wei Di
dihongweixs@163.com

¹ Engineering and Technology Research Center of Liupanshan Resources, College of Chemistry and Chemical Engineering, Ningxia Normal University, Guyuan 756000, China

magnesium hydroxide or aluminum hydroxide as flame retardant loses water when heated to generate magnesium oxide or aluminum oxide, which can be used as ceramifiable filler to kill two birds with one stone. However, magnesium oxide or aluminum oxide powder cannot be melted within 1000 °C, which destroys other ceramifiable inorganic fillers in the composite to form ceramic layer, resulting in poor ceramic strength. Therefore, it is impossible to achieve forming ceramics at low temperature with magnesium oxide or aluminum oxide as ceramifiable filler. The lack of high-performance ceramifiable flame-retardant polymer composites is increasingly becoming a development bottleneck of polymer composites for fire-resistant cables.

Melamine (MA) is a triazine nitrogen-containing heterocyclic organic compound. Melamine is the trimer of cyanamide, which will release a large amount of nitrogen when heated for decomposition, so it can be used as a vapor-phase flame retardant [12–14].

The research ideas of project applicants are as follows: EVA is used as polymer substrate; melamine (MA) is chosen as flame retardant because melamine belongs to gas-phase flame-retardant mechanism, and there is no residue after combustion, which will not damage the bending strength of ceramic products; organic montmorillonite (OMMT) as anti-dripping agent is also necessary to add; otherwise in the combustion process, the composite will melt and drip before the formation of ceramic. The ceramifiable inorganic filler is E-glass fiber (EGF); low softening phosphate glass powder (GP) is used as flux.

Experimental

Materials

EVA (Elvax 265) was provided by DuPont Company (USA). Melamine (MA) was supplied from Sinopharm Chemical Reagent Co., Ltd. (Shanghai, China). E-glass fiber (EGF) was provided by Radison Composites Co. Ltd. (Nanjing, China). Low softening phosphate glass powder (GP) was provided by Dong Gu New Materials Co. Ltd. (Feshan, China). OMMT (I.44P) was supplied from Nano Co. Ltd. (USA), which modifier is dioctadecyldimethylammonium chloride. The composition of investigated composites for EGF and GP is shown in Table 1.

Table 1 The composition of investigated composites

Part	SiO ₂ Ms%	CaO Ms%	Al ₂ O ₃ Ms%	MgO Ms%	Na ₂ O Ms%	Fe ₂ O ₃ Ms%	K ₂ O Ms%	TiO ₂ Ms%	P ₂ O ₅ Ms%	SO ₃ Ms%	ZnO Ms%	Others Ms%
EGF	58.14	24.20	13.33	2.88	0.46	0.34	0.34	0.24				0.07
GP	5.47	0.91	23.82		10.03	0.03	14.05	0.41	45.13	0.08	0.01	0.06

*Others: volatile compounds and minor oxides

Preparation of EVA composites sample

The ceramifiable EVA composites are consisting of EVA, MA, EGF, GP, and OMMT. Firstly, all raw materials were dried in a vacuum oven at 60 °C for 12 h. Then, the EVA composites with different ratios of additives were prepared by a twin-screw extruder (SA1200II, Haitian Plastics Machinery Group Co. Ltd., Nanjing, China) with a rotation speed of 150 rpm at the following temperature range from the feed zone to the die: 175, 180, 185, 185, 180, and 175 °C. The extruded products were pressed into different samples by plate vulcanizer (QingDao Yahua Machinery Co. Ltd., China) at 170 °C and cold-pressed at room temperature for 3 min.

Preparation of EVA composite-based ceramic

The ceramics were prepared by muffle furnace (KSL-1200X-J, Hefei Kejing Materials Technology Co. Ltd., China). EVA composites samples with the dimension of 30×4×3 mm were heated from room temperature to 700, 800, 900, and 1000 °C, respectively, at a heating rate of 10 °C min⁻¹.

Measurements

The UL-94 vertical burning level was tested on a vertical burning instrument (CZF-4, Nanjing, China) according to ASTM D3801, the dimensions of samples were 130 mm×13 mm×3.2 mm.

The LOI value was measured by an oxygen index instrument (HC-2C, Nanjing, China) according to ASTM D2863-97 with a sheet dimension of 130 mm×6.5 mm×3.2 mm.

The flexural strengths of EVA composite-based ceramics were measured via the 3-point bend method on a testing machine (CMT2000, SANS Inc., China) according to the procedure in GB 6569-2006, and the loading rate was 0.5 mm min⁻¹. All data are the average of five independent flexural strengths.

The flammability of the ceramifiable EVA composites was evaluated by a cone calorimeter (Fire Testing Technology, UK) according to ISO 5660-1 at a heat flux 50 kW m⁻². The samples were molded to size of 100 mm×100 mm×3 mm.

Thermal decomposition behavior of the ceramifiable EVA composite was conducted using a NETZSCH TGA (209 F1) with ± 0.1 °C temperature error at a heating rate of 10 °C min^{-1} under N_2 at a flow rate of 50 mL min^{-1} .

TG-IR was performed using TGA (STA8000+, PE, USA) that was linked to FTIR (Frontier, PerkinElmer, USA). The test was carried out from 30 to 700 °C at a heating rate of 10 °C min^{-1} under the nitrogen flow rate of 3×10^{-5} $\text{m}^3 \text{min}^{-1}$.

The morphology and elemental dispersion of EVA composite-based ceramics were characterized by SEM–EDX using a JSM-7610F SEM (JEOL, Japan) and a EDX system (OXFORD INCA250, UK) at an acceleration voltage of 15 kV. All samples are sprayed with gold layer before being examined.

X-ray diffraction (XRD) (SmartLab-SE, Rigaku Corporation, Japan) analysis was performed with an $\text{Cu-K}\alpha$ radiation in the range of $2\theta = 5\text{--}60^\circ$ with the step length of 0.06° at 40 kV.

Results and discussion

The flame retardancy of the ceramifiable flame-retarded EVA composites

The flame retardancy of the ceramifiable EVA composites was evaluated by UL-94 and LOI test, and the results are shown in Table 2. The corresponding vertical combustion test samples are shown in Fig. 1. As shown in Table 2, the addition of 5 Ms% OMMT to EVA/CF composite (sample 3) had the effect of anti-dripping. The composite without molten droplets provided a material basis for later ceramic transformation. To achieve the flame retardancy of EVA/



Fig. 1 Digital photographs of sample after UL-94 tests **a** sample 1; **b** sample 3; **c** sample 9; and **d** sample 10

CF/OMMT composite, MA was incorporated into EVA/CF/OMMT composite. When adding 28 Ms% MA, the vertical combustion test result of EVA/CF/MA/OMMT composite (sample 10) based on UL-94 standard passed V-0 rating, and the corresponding oxygen index value (LOI) reached 27.8% . Obviously, MA is an effective flame retardant for EVA/CF/OMMT composite. OMMT had a good flame-retardant synergistic effect on EVA/CF/MA composite, which is due to the exfoliated layered structure of OMMT can reduce the melt fluidity of polymer chains and promote the strength and density of EVA/CF/MA/OMMT composite carbon layer. We kept the proportion of EVA and CF unchanged, changed the proportion of OMMT from $0, 3$ to 7 , and the corresponding proportion of MA was $33, 30$, and 26 . As a result, these three formulas (samples 11, 12, and 13) had no flame-retardant rating. Obviously, the mass ratio of EVA/CF/MA/OMMT

Table 2 LOI and UL-94 data of EVA composites

Sample	EVA /Ms%	CF (GP:EGF = 7:3) /Ms%	OMMT /Ms%	MA /Ms%	UL-94	LOI /%
1	50	50	0	0	N.R./dripping	–
2	50	47	3	0	N.R./dripping	–
3	50	45	5	0	N.R./no dripping	–
4	40	45	5	10	N.R./no dripping	–
5	35	45	5	15	N.R./no dripping	–
6	35	40	5	20	N.R./no dripping	–
7	35	35	5	25	N.R./no dripping	–
8	35	35	0	30	N.R./dripping	–
9	35	32	0	33	N.R./dripping	–
10	35	32	5	28	V-0	27.8
11	35	32	0	33	N.R./dripping	–
12	35	32	3	30	N.R./dripping	–
13	35	32	7	26	N.R./no dripping	–

N.R.: no rating

is equal to 35/32/5/28, which should be the appropriate for the flame retardation of EVA composite.

Mechanical properties of the ceramics from EVA/CF/MA/OMMT composites formed at various temperatures

The flexural strength of EVA composite-based ceramics with various ratios of GP/EGF in ceramifiable fillers (CF) is shown in Table 3. At 700 °C, the flexural strength of ceramics increased with adding the ratio of GP/EGF until the ratio reached 7:3, and then, it descended with further adding the ratio of GP/EGF, the maximum is 5.1 MPa. At 800 °C, the flexural strength of ceramics has the same change trend as that occurred at 700 °C, the maximum is 10.6 MPa at 800 °C. However, the ratio of GP/EGF reduced while reaching the maximum flexural strength for the ceramic at 900 °C and 1000 °C, and the ratio values are 6/4 and 5/5, respectively, corresponding to the maximum 17.1 MPa at 900 °C and 22.3 MPa at 1000 °C. Obviously, EGF has an outstanding effect on the flexural strength for the EVA composite-based ceramics. In Table 3, the ratio of 7:3 (GP/EGF) is considered an appropriate value to fabricate the EVA composite-based ceramic if we consider forming the ceramic at low temperature.

Combustion performance of the ceramifiable flame-retarded EVA composite

Cone calorimeter (CC) is also an effective method to assess the flammability and combustion behavior of flame-retarded polymer composites. The heat release rate (HRR), the total release rate (THR), and the smoke production rate (SPR) with burning time of neat EVA and EVA composite are exhibited in Fig. 2. The corresponding data are summarized in Table 4. As shown in Fig. 2a, a very sharp peak of HRR for pure EVA appeared fastly, and the peak value (PHRR) is about 1226.9 kW m⁻². Compared with EVA, the PHRR of the EVA/CF and EVA/CF/OMMT composites has sharply decreased to 483.1 and 477.4 kW m⁻², respectively. This indicates that the addition of infinite fillers can effectively reduce the PHRR of EVA/CF composites. However, OMMT has little effect on further

reducing the PHRR. The PHRR of EVA/CF/MA/OMMT composite further significantly decreased to 306.8 Kw m⁻² on the basis of EVA/CF and EVA/CF/OMMT composites, indicating that the addition of flame-retardant MA can also effectively reduce the PHRR. Furthermore, the HRR curve of EVA/CF/MA/OMMT composite exhibits two peaks. The first peak is explained by the combustion of EVA composite. At the same time, the thermal insulation layer is formed; the second peak is attributed to the destruction of the carbonaceous inorganic structure layer.

Total heat release (THR) is an important index to estimate the fire security of materials. From Fig. 1b, THR of EVA/CF, EVA/CF/OMMT, and EVA/CF/MA/OMMT composites is obvious decline compared with the one of the neat EVA. The THR value for neat EVA is 114.3 MJ m⁻², while the THR value for EVA/CF, EVA/CF/OMMT, and EVA/CF/MA/OMMT composites is 100.8, 89.9, and 85.5 MJ m⁻², respectively. THR values also indicate that EVA/CF/MA/OMMT system has better flame retardancy.

Furthermore, the SPR curves of neat EVA and EVA composite are exhibited in Fig. 2c. As shown from Fig. 1c, a very sharp peak of SPR for pure EVA appeared fastly, and the peak value (PSPR) is about $9.9 \times 10^{-2} \text{ m}^2 \text{ s}^{-1}$. Compared to pure EVA, the PSPR of the EVA/CF and EVA/CF/OMMT composites has sharply decreased to 4.8×10^{-2} and $3.9 \times 10^{-2} \text{ m}^2 \text{ s}^{-1}$, respectively, which indicates that the addition of infinite fillers can effectively reduce the PSPR of EVA/CF composites. However, OMMT has little effect on further reducing the PSPR. The PSPR of EVA/CF/MA/OMMT composite further significantly decreased to $0.9 \times 10^{-2} \text{ m}^2 \text{ s}^{-1}$ on the basis of EVA/CF and EVA/CF/OMMT composites, indicating that the addition of flame-retardant MA can significantly reduce the PSPR. The reason for the low SPR of EVA/CF/MA/OMMT composite may be that the gases released by the decomposition of flame-retardant MA are water, carbon dioxide, and ammonia, not carbon particles (this conclusion was obtained from 3.5 TG-IR analysis). It is noticeable that the smoke suppression effect of EVA/CF/MA/OMMT composite is dramatically improved.

In brief, MA and OMMT contribute to the flame retardation of EVA.

Table 3 Flexural strength of ceramics

Composition/Ms%	Flexural strength/MPa			
	700 °C	800 °C	900 °C	1000 °C
EVA35/CF32 (GP:EGF = 5:5)/MA28/OMMT5	1.8 ± 0.3	6.9 ± 0.5	16.5 ± 0.9	22.3 ± 1.2
EVA35/CF32 (GP:EGF = 6:4)/MA28/OMMT5	3.9 ± 0.4	8.1 ± 0.7	17.1 ± 1.2	20.8 ± 1.0
EVA35/CF32 (GP:EGF = 7:3)/MA28/OMMT5	5.1 ± 0.6	10.6 ± 0.8	15.9 ± 1.1	18.5 ± 1.1
EVA35/CF32 (GP:EGF = 8:2)/MA28/OMMT5	4.6 ± 0.5	8.9 ± 0.9	13.7 ± 1.0	–

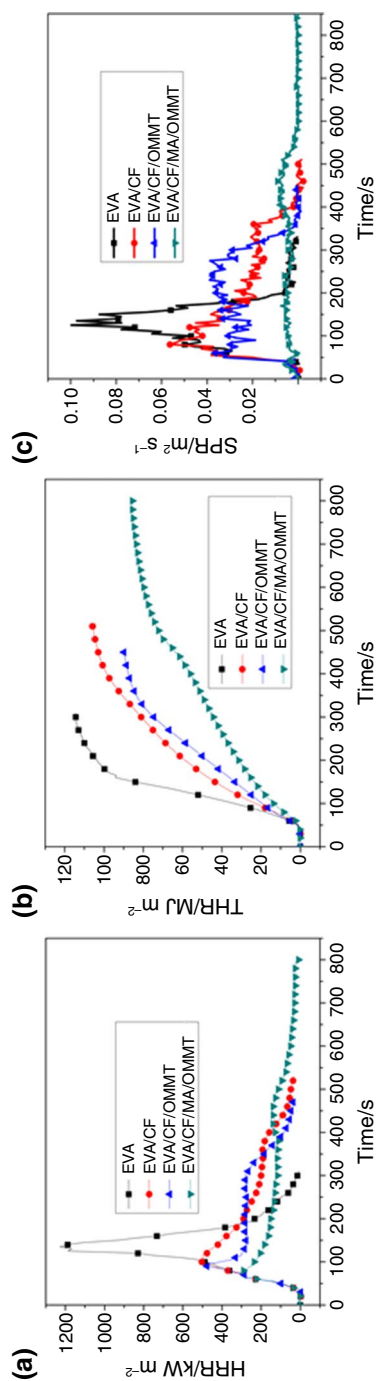


Fig. 2 HRR (a), THR (b), and SPR (c) curves of neat EVA and its composite in CC test

Thermal stability analysis of the ceramifiable flame-retarded EVA composite

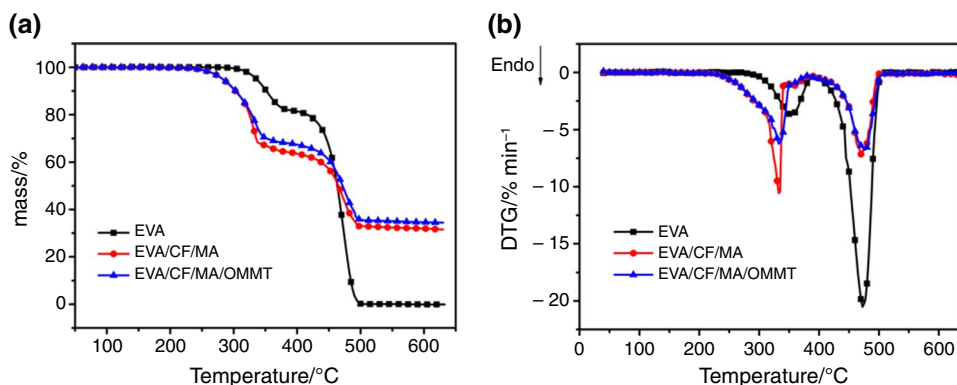
The thermal degradation behavior of the EVA composites was investigated in hope of finding the potential flame-retardant mode. Figure 3 shows the mass loss curves (TG), the derivative curves (DTG) of EVA, EVA35/CF35/MA30, and EVA35/CF32/MA28/OMMT5 composites under nitrogen atmosphere. The corresponding data are recorded in Table 5. Figure 3a shows that the thermal degradation of EVA underwent two steps (TG), clearly related to the two peaks of the DTG curve in Fig. 3b. The first step (300–400 °C) was attributed to the loss of acetic acid and the formation of the polyunsaturated chain along EVA backbone [15]. The first maximum mass losses occurred at 352.5 °C ($T_{\max 1}$). The second step (400–500 °C) was caused by the polyunsaturated chains scission of the polymeric main chain and the volatilization of the carbonaceous residue [16]. In this step, $T_{\max 2}$ is 472.5 °C. The thermal decomposition of the EVA composites has three steps. For EVA35/CF35/MA30 composite, the first degradation step (230–340 °C) with a maximum degradation rate at 332.5 °C ($T_{\max 1}$) was mainly attributed to the sublimation and its thermal dissociation of MA besides the decomposition of EVA side chain. The second decomposition step with a maximum degradation rate at 360.0 °C ($T_{\max 2}$) was caused by the thermal degradation of EVA side chain. The third degradation step with a maximum degradation rate at 470.0 °C ($T_{\max 3}$) should be due to the polyunsaturated chains scission of the polymeric backbone, the further thermal degradation of MA, and the volatilization of the carbonaceous residue formed before. From the thermal analysis results of EVA35/CF35/MA30 composite compared with EVA, we believed that flame-retardant MA promotes the decomposition and carbonization of EVA. For EVA35/CF32/MA28/OMMT5 composite, its $T_{\max 1}$ (332.7 °C), $T_{\max 2}$ (360.2 °C), $T_{\max 3}$ (477.5 °C) increased by 0.2 °C, 0.2 °C, and 7.5 °C, respectively, compared with EVA35/CF35/MA30 composite after adding 5% OMMT, indicating that adding OMMT can improve the thermal stability of the material. The intercalated structure of OMMT can promote the stability of carbon layer, and the stable carbon layer can hinder the EVA further decomposition, resulting in the higher thermal stability of EVA/CF/MA/OMMT composite than EVA/CF/MA composite in the three thermal decomposition stages. From above, EVA/CF/MA/OMMT composite has better flame retardancy than that of EVA/CF/MA composite.

TG-IR analysis of the ceramifiable flame-retarded EVA composite

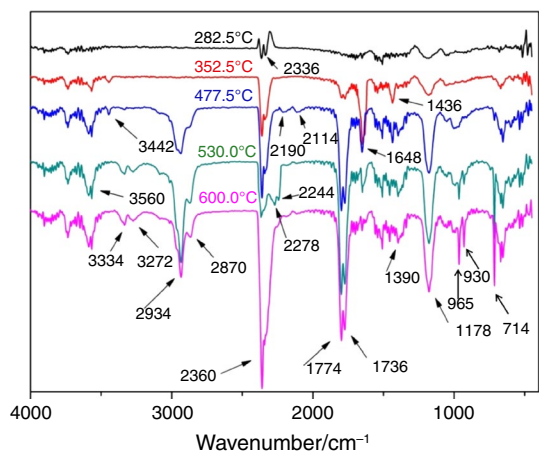
In order to further explore the flame-retardant mechanism of EVA/CF/MA/OMMT composite, this work was carried out

Table 4 CC data of EVA and EVA composite

Composition/Ms%	PHRR/kW m ⁻²	THR/MJ m ⁻²	PSPR/1 × 10 ⁻² m ² s ⁻¹
EVA	1226.9	114.3	9.9
EVA50/CF50	483.1	100.8	4.8
EVA50/CF45/OMMT5	477.4	89.9	3.9
EVA35/CF32/MA28/OMMT5	306.8	85.5	0.9

Fig. 3 TGA (a) and DTG (b) curves of EVA and EVA composites in nitrogen**Table 5** TGA and DTG data of EVA and EVA composites in nitrogen

Composition/Ms%	T _{5%} /°C	T _{max1} /°C	T _{max2} /°C	T _{max3} /°C	Residues at 800 °C / Ms%
EVA	333.7	352.5	472.5	–	0
EVA35/CF35/MA30	282.5	332.5	360.0	470.0	33.6
EVA35/CF32/MA28/OMMT5	282.5	332.7	360.2	477.5	35.3

**Fig. 4** TG-IR curves of the ceramifiable flame-retarded EVA composite in nitrogen

by TG-IR test method, which enables us to understand the contribution of volatile products of EVA/CF/MA/OMMT composite to the flame-retardant performance at different temperatures. Figure 4 shows the infrared characteristic

peaks of volatile products of EVA/CF/MA/OMMT composite at different temperatures. There are almost no infrared characteristic peaks at 282.5 °C. The infrared characteristic peaks at 352.5 °C (the first maximum mass loss rate temperature of EVA/CF/MA/OMMT composite) correspond to water vapor (H₂O: 4000–3560 cm⁻¹) [17–19]; carbon dioxide (CO₂: 2336 and 2360 cm⁻¹) [20, 21]; melamine (C₃H₆N₆: 3442, 1648 and 1436 cm⁻¹) [17, 22, 23], which is due to the sublimation of melamine; carboxylic acid ester (1774, 1736, and 1178 cm⁻¹) [21, 24]; and 1390 cm⁻¹ is C–H deformation vibration of CH₃ in acetic acid [21], which is the carboxylic acid decarboxylation of EVA. The characteristic peak of aliphatic hydrocarbon (2934 and 2870 cm⁻¹) [17, 21] was observed at 477.5 °C (the second maximum mass loss rate temperature corresponding of EVA/CF/MA/OMMT composite), which was mainly caused by the main chain break of EVA. The infrared characteristic peak of CO (2190 and 2114 cm⁻¹) [25–27] was also observed at 477.5 °C. The infrared characteristic peak of HOCN (2278 and 2244 cm⁻¹) [25, 28] and NH₃ (965 and 930 cm⁻¹) [29, 30], HCN (3334, 3272 and 714 cm⁻¹) [30, 31] was also observed at 530 °C, mainly due to the further thermal

decomposition of melamine. It can be seen that the infrared characteristic peak of CO_2 , H_2O , NH_3 , HCN , carboxylic acid, and aliphatic hydrocarbon appears at 600°C . It should be noted that during heating or combustion, the release of non-combustible gas products (CO_2 , NH_3 , and H_2O) is synchronized with the combustible gas products (carboxylic acid, CO , and aliphatic hydrocarbon), the combustible gas products are diluted, and the combustion effect is significantly decreased. The gas-phase flame retardance mechanism is shown in Fig. 5. Thermal sublimation and decomposition of MA is shown in Scheme 1. Flame-retardant MA sublimates or decomposes into gas when heated, and there is no solid residue of flame retardant inside the ceramic, which does not affect the strength of the ceramic.

Morphologies of the EVA composite-based ceramics formed at various temperatures

Cross-sections of the EVA composite-based ceramics formed at various temperatures are shown in Fig. 6. As shown from Fig. 6, the ceramic cross-section has holes due to the decomposition of flame-retardant MA and EVA to produce gases, some of which remain inside the ceramic to form porous ceramics. In Fig. 6a, GP at 700°C has been melted and then cooled to form the solidified phase. In this case, the temperature is not high enough

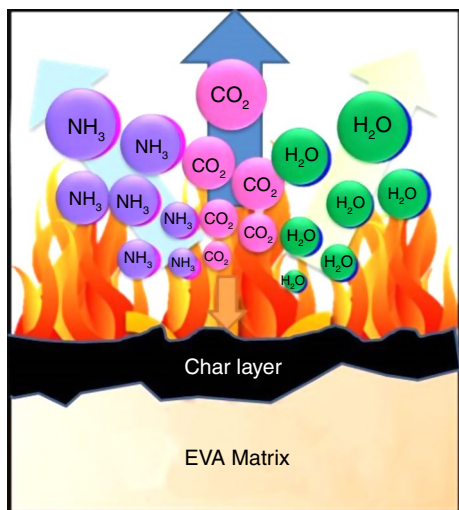
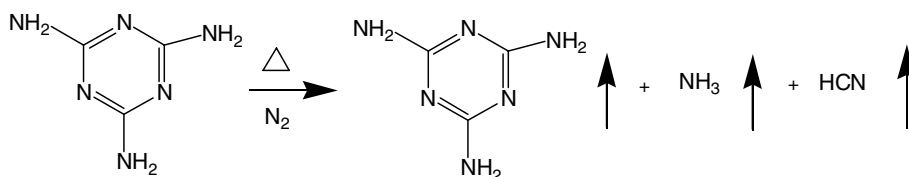


Fig. 5 Schematic diagram of melamine vapor-phase flame-retardant mechanism

Scheme 1 Thermal sublimation and decomposition of melamine

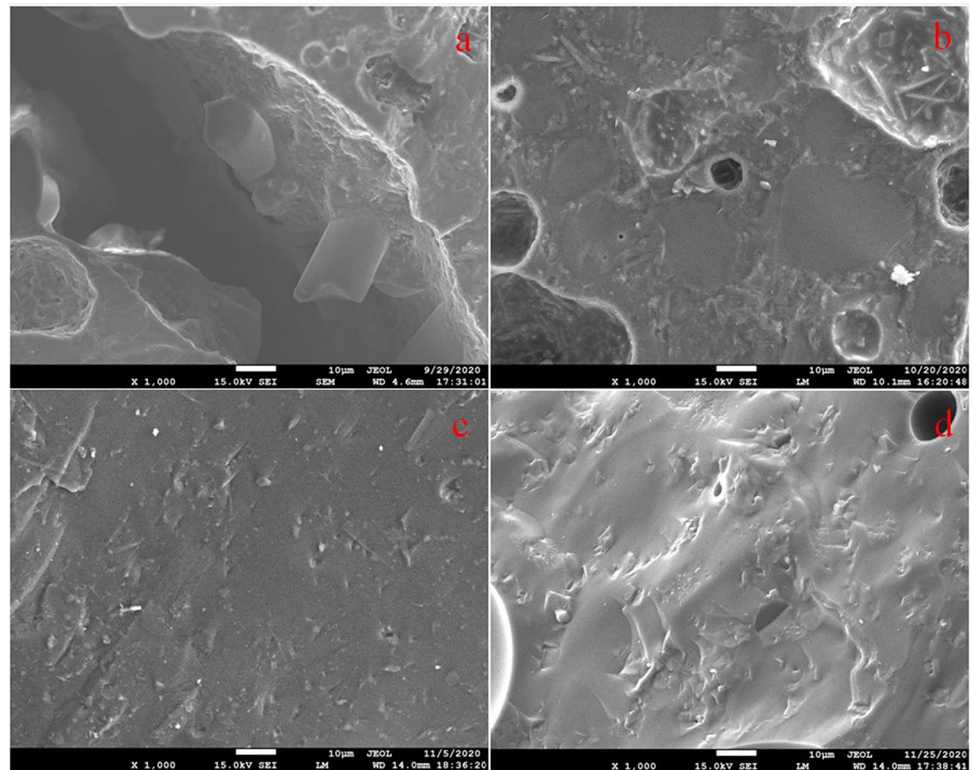


to make EGF melted. EGF is mostly isolated, and interface between EGF and GP is obvious, which indicates that liquidity of liquid phase from GP at 700°C is not enough to fully penetrate the internal of EGF. That is to say, EGF is not completely coated by liquid phase. In contrast, the interface between EGF and GP is more and more blurred, and the EGF particles are shown in Fig. 6b, the interface almost disappeared in Fig. 6c and d, which demonstrate that more liquid phase with high-flow ability can partially penetrate or fully penetrate the internal of EGF, and EGF is fully coated, with the increase in temperature. Meanwhile, EGF may eutectic react with GP on heating, which has been confirmed by XRD test results. The eutectic can form in the interface of EGF and GP, which can decrease the melting point of EGF, and EGF melt below 1000°C . This eutectic liquid acts as a micro-bridges between EGF and GP, and the bonding between EGF and GP is more advanced, improving the strength of the ceramic.

XRD analysis

XRD pattern of EVA composite-based ceramics formed at different temperatures, GP and EGF, respectively, are shown in Fig. 7. Because GP and EGF are both amorphous phases, GP (Fig. 7a) and EGF (Fig. 7b) have only diffuse diffraction peaks of amorphous phase at $2\theta = 20 \sim 40^\circ$. Figure 7c–f shows that there are not only diffuse diffraction peaks of amorphous phase at $2\theta = 20 \sim 40^\circ$, but also characteristic peaks of $\text{K}(\text{AlSi}_3\text{O}_8)$, cristobalite, and wollastonite crystals in ceramic samples at $700\text{--}800^\circ\text{C}$ [2, 4, 8]. At 900°C , the characteristic peaks of $\text{K}(\text{AlSi}_3\text{O}_8)$ crystals disappear, which indicates that the phosphate that is not easy to crystallize in GP gradually destroys the silicate crystal structure that is easy to crystallize in EGF. At 1000°C , there are new crystals peaks such as MgSiO_3 [2, 4] except for the characteristic peaks of cristobalite. The existence of these crystal characteristic peaks indicates that the eutectic reaction between GP and EGF occurs in the ablation process and forms the eutectic phase. This shows that with the increase in temperature, GP and EGF continue to fuse, and the original crystal structure is destroyed and a new crystal structure is generated. The ceramic process schematic diagram of ceramifiable polymer composites is shown in Fig. 8.

Fig. 6 SEM micrographs of ceramics obtained at different temperatures **a** sample at 700 °C; **b** sample at 800 °C; **c** sample at 900 °C; and **d** sample at 1000 °C



Conclusions

In this work, a joint MA/OMMT as a novel flame retardant was developed to achieve the highly efficient flame retardance and ceramization of EVA/CF/MA/OMMT composite. The flame-retardant test results demonstrated that when

EVA/CF (GP:EGF)/MA/OMMT = 35/32 (7:3)/28/5, EVA composite reached V-0 rating (UL-94), and the corresponding LOI is 27.8. The cone calorimetric test results illustrated that HRR, THR, and SPR of the EVA composite were significantly lower than neat EVA. TG-IR test results confirmed that a large amount of incombustible gases from melamine

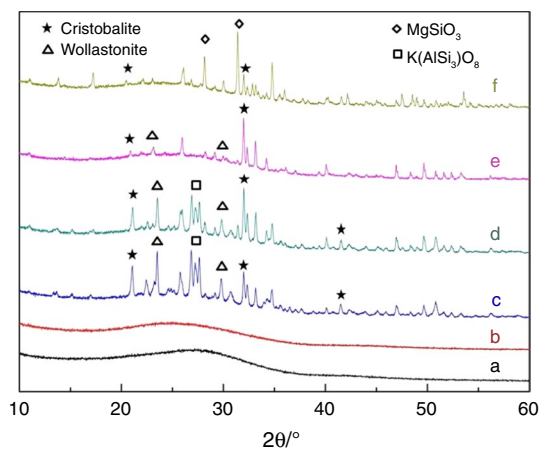


Fig. 7 XRD of the ceramics formed at different temperatures **a** GP; **b** EGF; **c** the ceramic formed at 700 °C; **d** the ceramic formed at 800 °C; **e** the ceramic formed at 900 °C; and **f** the ceramic formed at 1000 °C

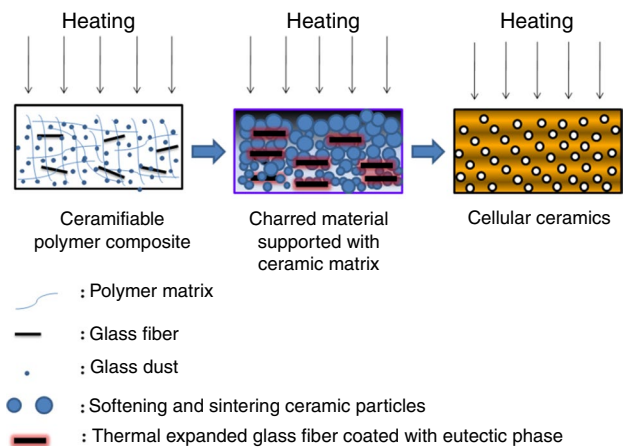


Fig. 8 Schematic diagram of ceramic process

thermal decomposition diluted the combustible gases produced by EVA decomposition, which is the reason why EVA composite has good flame retardancy. Bending strength test results showed that the flexural strength for the EVA composite-based ceramic formed at 700 °C reached 5.1 MPa. The bending strength of ceramics fired at 1000 °C reached the maximum value of 18.5 Mpa. SEM and SEM–EDX analysis in mapping mode and XRD analysis illustrated that the molten GP and EGF had eutectic react at the two-phase interface and formed a new liquid phase. The eutectic liquid phase gradually diffused or penetrated into EGF, which played a role of bridging and adhesion. The formed eutectic liquid phase objectively reduced the softening point of EGF, which made EGF gradually melting, partially disappeared, and finally completely disappeared. All these results demonstrated that an efficient ceramifiable flame-retarded EVA composite was prepared successfully.

Funding The funding was provided by Science and Technology Support Plan Project of Ningxia, China, NKJZ [2015] No. 26 Document, The First-rate Discipline (Education) Construction Project of the Higher Education Institutions of Ningxia, China, No. NXYLXK2017B11, Engineering and Technology Research Center of Liupanshan Resources Grant, and Ningxia Normal University, China, No. HGZD19-03, and Natural Science Foundation of Ningxia, China, 2020AAC03261.

References

- Li YM, Deng C, Zhao ZY, et al. Carbon fiber-based polymer composite via ceramization toward excellent electromagnetic interference shielding performance and high temperature resistance. *Compos A Appl Sci Manuf*. 2020. <https://doi.org/10.1016/j.compositesa.2020.105769>.
- Yang J, Xu Y, Jiang W, et al. The thermal transformation process and mechanical strength evolution of ceramifiable silicone composites. *Ceram Int*. 2021. <https://doi.org/10.1016/J.CERAMINT.2021.04.134>.
- Song J, Huang Z, Qin Y, et al. Effects of zirconium silicide on the vulcanization, mechanical and ablation resistance properties of ceramifiable silicone rubber composites. *Polymers*. 2020. <https://doi.org/10.3390/polym12020496>.
- Guo J, Gao W, Wang Y, et al. Effect of glass frit with low softening temperature on the properties, microstructure and formation mechanism of polysiloxane elastomer-based ceramizable composites. *Polym Degrad Stab*. 2017. <https://doi.org/10.1016/j.polymdegradstab.2016.12.012>.
- Guo J, Zhang Y, Li H, et al. Effect of the sintering temperature on the microstructure, properties and formation mechanism of ceramic materials obtained from polysiloxane elastomer-based ceramizable composites. *J Alloy Compd*. 2016. <https://doi.org/10.1016/j.jallcom.2016.04.030>.
- Hu S, Chen F, Li JG, et al. The ceramifying process and mechanical properties of silicone rubber/ammonium polyphosphate/aluminium hydroxide/mica composites. *Polym Degrad Stab*. 2016. <https://doi.org/10.1016/j.polymdegradstab.2016.02.010>.
- Imiela M, Anyszka R, Bieliński DM, et al. Effect of carbon fibers on thermal properties and mechanical strength of ceramifiable composites based on silicone rubber. *J Therm Anal Calorim*. 2016. <https://doi.org/10.1007/s10973-015-5115-x>.
- Anyszka R, Bieliński DM, Pędzich Z, et al. Effect of mineral filler additives on flammability, processing and use of silicone-based ceramifiable composites. *Polym Bull*. 2018. <https://doi.org/10.1007/s00289-017-2113-0>.
- Lou F, Wu K, Wang Q, et al. Improved flame-retardant and ceramifiable properties of EVA composites by combination of ammonium polyphosphate and aluminum hydroxide. *Polymers*. 2019. <https://doi.org/10.3390/polym11010125>.
- Zhao D, Shen Y, Wang T. Ceramifiable EVA/APP/SGF composites for improved ceramifiable properties. *Polym Degrad Stab*. 2018. <https://doi.org/10.1016/j.polymdegradstab.2018.02.006>.
- Li YM, Deng C, Long JW, et al. Improving fire retardancy of ceramifiable polyolefin system via a hybrid of zinc borate@ melamine cyanurate. *Polym Degrad Stab*. 2018. <https://doi.org/10.1016/j.polymdegradstab.2018.05.012>.
- Price D, Liu Y, Milnes GJ, et al. An investigation into the mechanism of flame retardancy and smoke suppression by melamine in flexible polyurethane foam. *Fire Mater*. 2002. <https://doi.org/10.1002/fam.810>.
- Zhou R, Mu J, Sun X, et al. Application of intumescent flame retardant containing aluminum diethyphosphinate, neopentyl glycol, and melamine for polyethylene. *Saf Sci*. 2020. <https://doi.org/10.1016/j.ssci.2020.104849>.
- Xu W, Wang G, Xu J, et al. Modification of diatomite with melamine coated zeolitic imidazolate framework-8 as an effective flame retardant to enhance flame retardancy and smoke suppression of rigid polyurethane foam. *J Hazard Mater*. 2019. <https://doi.org/10.1016/j.jhazmat.2019.120819>.
- Zhang Z, Du J, Shi M. Quantitative analysis of the calcium hydroxide content of EVA-modified cement paste based on TG-DSC in a dual atmosphere. *Materials*. 2022. <https://doi.org/10.3390/MA15072660>.
- Qian Y, Li S, Chen X. Preparation of mesoporous silica-LDHs system and its coordinated flame-retardant effect on EVA. *J Therm Anal Calorim*. 2017. <https://doi.org/10.1007/s10973-017-6508-9>.
- Hu X, Li M, Yang J, et al. In situ fabrication of melamine hydroxy ethylidene diphosphonate wrapped montmorillonite for reducing the fire hazards of epoxy resin. *Appl Clay Sci*. 2021. <https://doi.org/10.1016/J.CLAY.2020.105934>.
- Yang W, Song L, Hu Y, Lu H, Yuen RKK. Investigations of thermal degradation behavior and fire performance of halogen-free flame retardant poly(1,4-butylene terephthalate) composites. *J Appl Polym Sci*. 2011. <https://doi.org/10.1002/app.34119>.
- Wang Y, Yuan J, Ma L, Yin X, Zhu Z, Song P. Fabrication of anti-dripping and flame-retardant polylactide modified with chitosan derivative/aluminum hypophosphite. *Carbohydr Polym*. 2022. <https://doi.org/10.1016/J.CARPOL.2022.120141>.
- Chen X, Huo L, Jiao C, et al. TG–FTIR characterization of volatile compounds from flame retardant polyurethane foams materials. *J Anal Appl Pyrol*. 2013. <https://doi.org/10.1016/j.jaap.2012.12.017>.
- Guo Y, Liu J, Luo J, et al. Enhancement of thermal stability and flame retardancy of ethylene vinyl acetate/magnesium hydroxide composite by carbon black. *Fire Mater*. 2022. <https://doi.org/10.1002/fam.3093>.
- Cong X, Sun X, Ning B. Could infrared spectroscopy identify melamine-related stone using melamine-contained mixture as a reference? *J Clin Lab Anal*. 2013. <https://doi.org/10.1002/jcla.21562>.
- Mircescu NE, Oltean M, Chiş V, et al. FTIR, FT-Raman, SERS and DFT study on melamine. *Vib Spectrosc*. 2012. <https://doi.org/10.1016/j.vibspec.2012.04.008>.

24. Jia C, Chen X, Qian Y. Synergistic flame retardant effect of graphite powder in EVA/LDH composites. *Plast, Rubber Compos*. 2014. <https://doi.org/10.1179/1743289813Y.0000000072>.
25. Yang W, Song L, Hu Y, et al. Enhancement of fire retardancy performance of glass-fibre reinforced poly (ethylene terephthalate) composites with the incorporation of aluminum hypophosphite and melamine cyanurate. *Compos B Eng*. 2011. <https://doi.org/10.1016/j.compositesb.2011.03.019>.
26. Li L, Qian Y, Jiao CM. Synergistic flame retardant effect of melamine in ethylene–vinyl acetate/layered double hydroxides composites. *J Therm Anal Calorim*. 2013. <https://doi.org/10.1002/pen.23619>.
27. Chen X, Ma C, Jiao C. Synergistic effects between iron–graphene and melamine salt of pentaerythritol phosphate on flame retardant thermoplastic polyurethane. *Polym Adv Technol*. 2016. <https://doi.org/10.1002/pat.3823>.
28. Yang W, Lu H, Tai Q, et al. Flame retardancy mechanisms of poly (1, 4-butylene terephthalate) containing microencapsulated ammonium polyphosphate and melamine cyanurate. *Polym Adv Technol*. 2011. <https://doi.org/10.1002/pat.1735>.
29. Hu JP, Li D, Qin Y, et al. Promotion effect of melamine on flame retardancy of epoxy resins containing caged bicyclic phosphate. *Chin J Polym Sci*. 2007. <https://doi.org/10.1142/s0256767907002497>.
30. Jiang Y, Zhou W, Jiang M, et al. Flame retardant study of formalized polyvinyl alcohol fiber coated with melamine formaldehyde resins and the synergistic effect of copper ions. *Polym Degrad Stab*. 2017;144:331–43. <https://doi.org/10.1016/j.polymdegradstab.2017.08.014>.
31. Xu D, Yu K, Qian K. Thermal degradation study of rigid polyurethane foams containing tris (1-chloro-2-propyl) phosphate and modified aramid fiber. *Polym Test*. 2018;67:159–68. <https://doi.org/10.1016/j.polymertesting.2018.01.034>.

Publisher's Note Springer Nature remains neutral with regard to jurisdictional claims in published maps and institutional affiliations.

Springer Nature or its licensor (e.g. a society or other partner) holds exclusive rights to this article under a publishing agreement with the author(s) or other rightsholder(s); author self-archiving of the accepted manuscript version of this article is solely governed by the terms of such publishing agreement and applicable law.